Available online at www.sciencedirect.com
ScienceDirect
Polymer 49 (2008) 1356–1364
polymer
www.elsevier.com/locate/polymer

Polymer transcrystallinity induced by carbon nanotubes

Shanju Zhang [a], Marilyn L. Minus [a], Lingbo Zhu [b], Ching-Ping Wong [b], Satish Kumar [a,*]

[a] School of Polymer, Textile and Fiber Engineering, Georgia Institute of Technology, 801 Ferst Drive, Atlanta, GA 30332, United States
[b] School of Materials Sciences and Engineering, Georgia Institute of Technology, 771 Ferst Drive, Atlanta, GA 30332, United States

Received 4 December 2007; received in revised form 19 December 2007; accepted 5 January 2008
Available online 16 January 2008

Abstract

In this work, we provide the evidence of polymer transcrystallinity in the presence of carbon nanotubes (CNTs). The interfacial morphology of carbon nanotube fiber–polypropylene matrix is investigated by means of polarized optical microscopy (POM), wide-angle X-ray diffraction (WAXD), scanning electron microscopy (SEM) and transmission electron microscopy (TEM). The supramolecular microstructures of polypropylene transcrystals induced by the nanotube fiber are observed in the range of isothermal crystallization temperatures from 118 °C to 132 °C. The dynamic process of transcrystallization is analyzed by using the theory of heterogeneous nucleation. Microstructure analysis shows that the nanotubes can nucleate the growth of both α- and γ-transcrystal, and α-transcrystals dominate the overall interfacial morphology. Close to the nanotube fiber surface, a cross-hatched lamellar microstructure composed of mother lamellae and daughter lamellae is observed.

Keywords: Carbon nanotubes; Polymer transcrystallization; Interfacial structures

1. Introduction

Carbon nanotubes (CNTs) have been considered as a highly prospective reinforcing agent in the polymer matrix for future structural materials as they have large aspect ratio, very high strength, stiffness and flexibility [1–5]. However, their practical application as structural reinforcing fillers critically depends on the effective interfacial load transfer from the polymer matrix to the CNTs. It has been reported that the interfacial morphology plays a crucial role in enhancing load transfer [6–9]. Computer simulation and experimental observations have shown that strong interfacial strengths can be obtained by introducing chemical or physical bonding between CNTs and polymers [6–9].

Carbon fibers are used to reinforce polymers [10–16] and act as heterogeneous nucleating agent for polymer crystallizing along the interface with high nuclei density. These dense nuclei force the crystal growth normal to the carbon fiber axis. The resulting oriented crystalline layer is called transcrystalline layer [16]. Molecular orbital calculations show that helical conformation of α-form polypropylene with a monoclinic crystal lattice can be placed on a graphite lattice with all hydrogen atoms on the graphite surfaces [12]. At the molecular level, the polymer chains within the transcrystalline layer are parallel to the fiber axis [12]. Single-fiber pull-out experiments have shown that transcrystalline microstructures increase effective adhesion and stress transfer across the interface [17–19].

CNT-induced polymer crystallization has been studied in many polymers such as polypropylene, polyethylene, polyacrylonitrile and poly(vinyl alcohol) [20–24]. Periodic lamellar crystals of polyethylene along CNTs have been reported and the epitaxy between polyethylene and CNTs has been recognized [22]. However, to the best of our knowledge, there are no reports of polymer transcrystallization induced by CNTs to date. In this work, we report polypropylene transcrystallinity on the CNTs by controlled melt crystallization.

2. Experimental

Water-assisted CVD synthesis was performed in a horizontal alumina tube (3.8 cm diameter; 92 cm long) housed in

* Corresponding author. Tel.: +1 404 894 7550; fax: +1 404 894 8780.
E-mail address: satish.kumar@ptfe.gatech.edu (S. Kumar).

0032-3861/$ - see front matter © 2008 Elsevier Ltd. All rights reserved.
doi:10.1016/j.polymer.2008.01.018

a Lindberg Blue furnace [25]. The substrates used in this study were (001) silicon wafers coated with SiO_2 (500 nm) by thermal oxidation. The catalyst layers of Al_2O_3 (15 nm)/Fe (2 nm) were formed on the silicon wafer by sequential e-beam evaporation. CVD growth of CNTs was carried out at 750 °C with ethylene (150 sccm) as the carbon source, and hydrogen (180 sccm) and argon (350 sccm) as carrier gases. The water vapor concentration in the CVD chamber was controlled at 775 ppm by bubbling a small amount of argon gas through water. The resultant carbon nanotubes were multi-walled with an average 10 nm diameter and 1.0 mm length.

The as-produced CNTs were dispersed at a concentration of 0.5–1.0 wt% in polypropylene glycol by mechanical mixing. This dispersion was loaded into a 50 mm long syringe and subsequently ejected into a coagulation bath of diethyl ether using a syringe pump. Polyglycol dissolved in ether rapidly, leaving the formed nanotube fibers. The CNT fibers were collected on a winder and allowed to dry in air. To remove dope and coagulation solvents completely, the CNT fibers were heat-treated at 900 °C under nitrogen without tension for 1 h in a box furnace (Lindburg, 51668-HR Box Furnace 1200C, Blue M. Electric). The average diameter of CNT fibers is ca. 40 μm.

The matrix polymer used in this work was commercial grade isotactic polypropylene, PH835, with a melt flow index of 34.0 g/10 min and melting temperature of 165 °C, marketed by Basell. Commercial isotactic polypropylene was about 96% isotactic. The CNT fibers were placed between two polypropylene thin films and hot pressed at 200 °C to form a sandwich composite. The specimens were maintained at 200 °C for 5 min to erase thermal history of the sample and then cooled at a rate of 20 °C/min to the desired isothermal crystallization temperature. The resultant composite films had 50–100 μm thickness. Isothermal crystallization kinetics was studied under cross-polars in the temperature range from 118 °C to 132 °C on a Leica DMRX optical microscope equipped with a hot-stage (Linkam, THM-600). The Sony DKC-5000 video camera was used to record the images at regular time intervals.

For scanning electron microscopic (SEM) observation, the specimens were etched [26] for 1 h with a 1.0 wt% solution of potassium permanganate in a 2:1 mixture of concentrated sulphuric acid and phosphoric acid in an ultrasonic bath at room temperature. After the etching, the specimens were sequentially washed in dilute sulphuric acid, distilled water and acetone. The etched and washed specimens were dried at room temperature and then coated with a fine gold layer by ion-sputtering for examination in the SEM (LEO 1530) operated at 5 kV. Transmission electron microscopy (TEM) was done on Hitachi HF2000 operated at 120 kV.

Two-dimensional wide-angle X-ray diffraction (2-D WAXD) patterns were obtained in a transmission mode on Rigaku Micromax-002 ($\lambda = 0.15418$ nm) using Rigaku R-axis IV ++ detection system. All X-ray data were corrected for background (air and instrument) scattering before analysis. The diffraction patterns were analyzed using AreaMax V.1.00 and MDI Jade 6.1.

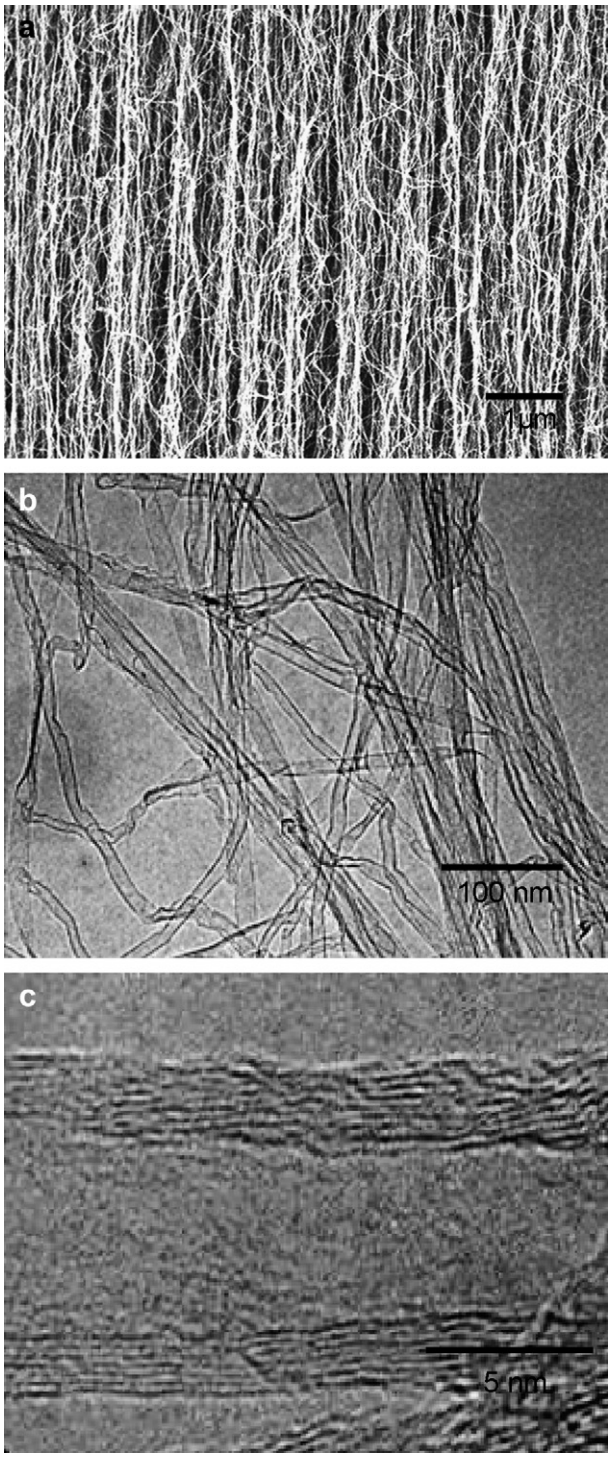

Fig. 1. One millimeter long multi-walled carbon nanotubes synthesized by water-assisted CVD method: (a) side wall; TEM bright field images of (b) nanotube arrays and (c) an individual nanotube.

The mechanical properties of the specimens were determined using RSA III solids analyzer (Rheometric Scientific, Co.) at room temperature. The thin films were cut to produce rectangular geometry for mechanical measurements. The displacement was determined by a controlled speed of 0.05 mm/min with a gauge length of 12.5 mm. For each experiment, at least three samples were tested.

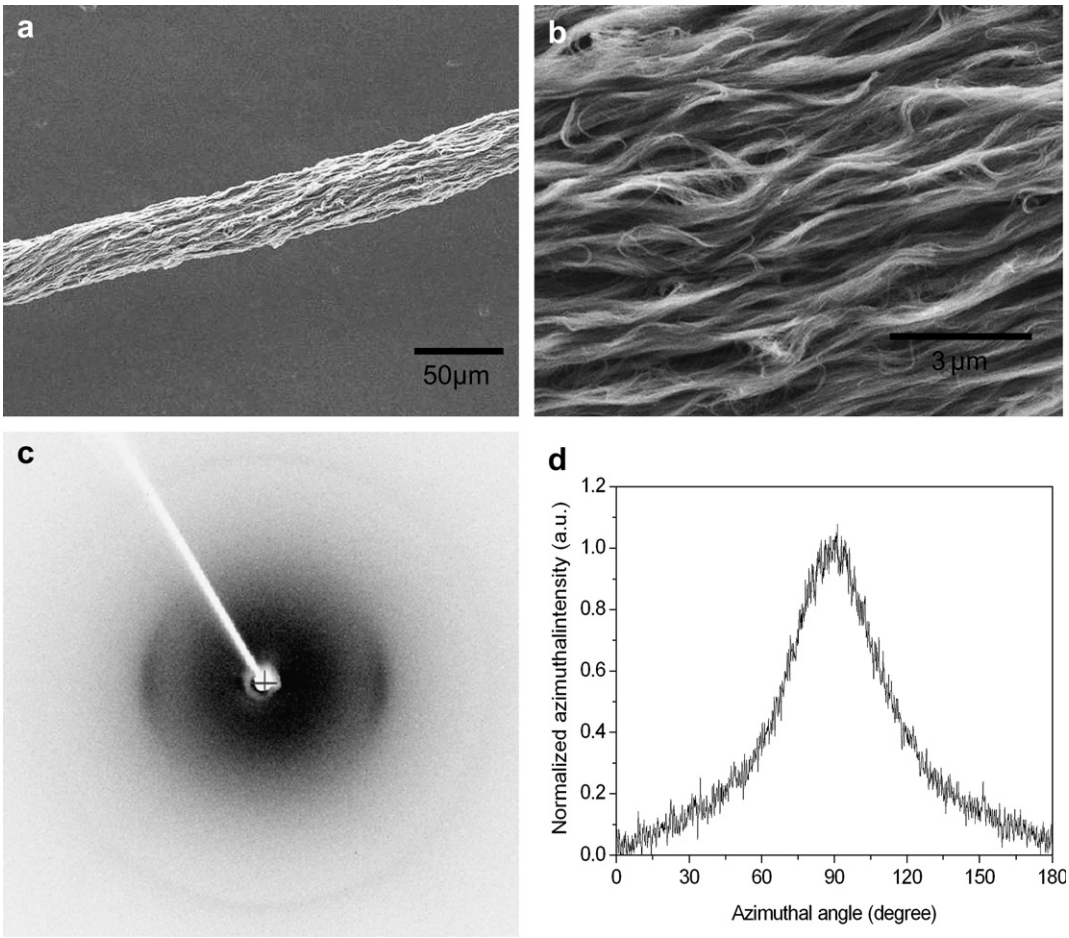

Fig. 2. (a) Low and (b) high magnification SEM images of a CNT fiber; (c) WAXD pattern with fiber axis vertical, and (d) (002) azimuthal intensity scan.

3. Results and discussion

In this work, CNTs contain 5–7 walls, which have an average 10 nm diameter and 1.0 mm length based on the SEM and TEM images (Fig. 1). The 2-D WAXD pattern of CNT fibers shows Bragg diffraction on the equator at $2\theta = 25.7^\circ$, corresponding to the graphite (002) plane in the CNTs. The (002) azimuthal intensity distribution gives carbon nanotube Herman's orientation factor of 0.49 (Fig. 2).

Fig. 3 shows typical polypropylene morphologies around the CNT fiber in the quiescent melt at 125 °C. The images show oriented crystalline lamellae surrounding the CNT fiber. This supramolecular structure is identified as the transcrystalline interphase [16]. Away from the CNT fiber, the polypropylene spherulites are observed. The impingement lines of the transcrystalline interphase and bulk spherulites are also observed. When two CNT fibers are close to each other, the area between two CNT fibers consists almost exclusively of transcrystalline interphases (Fig. 3b).

Fig. 4 shows a series of optical images taken at 122 °C with different crystallization times. Polypropylene nucleation first occurred at the surface of the CNT fiber within 30 s (Fig. 4a). This uniform transcrystalline growth front indicates the high nucleating ability of the CNT fiber toward the matrix. When the crystallization time approached 1 min, the spherulite nuclei in the polypropylene matrix were also observed (Fig. 4b), which grew into bulk spherulites (Fig. 4c–f). The growth direction of transcrystals is normal to the CNT fiber axis. This growth is ultimately hindered by the impingement with bulk spherulites or by another transcrystal (Fig. 4c–f).

Transcrystallization kinetics was studied in the 118–132 °C temperature range. Fig. 5a shows the growth of the transcrystals as a function of crystallization time at different temperatures. Growth rates at different temperatures were obtained from the slopes shown in Fig. 5a. According to the theory of heterogeneous nucleation [27], the growth rate (G) is expressed by Eq. (1).

$$G = G_0 \exp(-\Delta U/kT) \exp\left(-K_g/(T\Delta T)\right) \quad (1)$$

where G_0 is a constant, ΔU is the activation energy of chain motion in the melt, k is Boltzmann's constant, T is the crystallization temperature, ΔT, $T_m^0 - T$, is the supercooling degree (T_m^0 is the equilibrium melting temperature) and K_g is nucleation parameter. This nucleation parameter K_g represents the

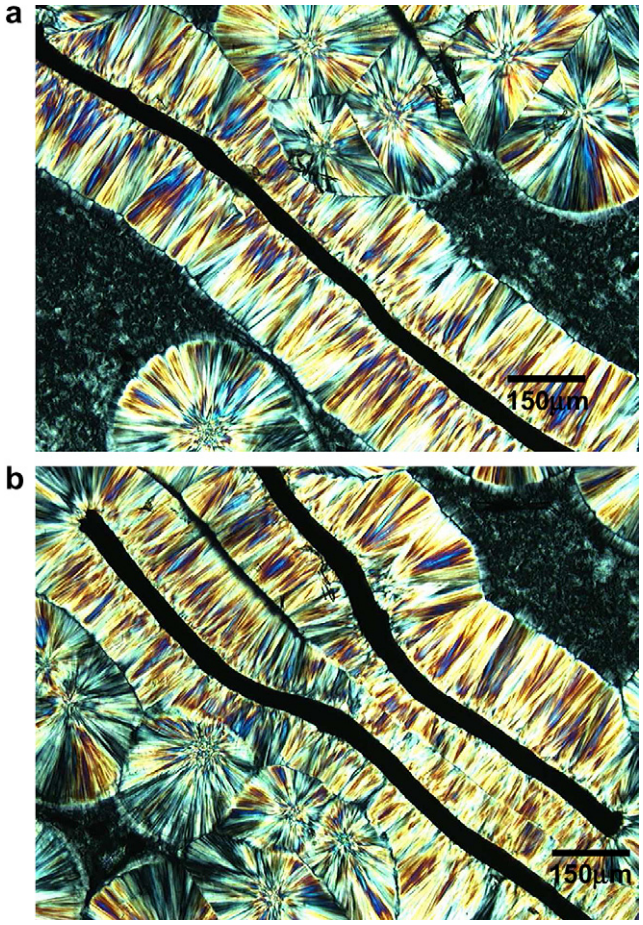

Fig. 3. Optical micrographs of transcrystalline interphases for polypropylene surrounding the CNT fibers isothermally crystallized at 125 °C: (a) a single CNT fiber and (b) two CNT fibers.

probability that a nucleus will reach the critical size and is determined by Eq. (2).

$$K_g = 4b_0\sigma_s\sigma_e T_m^0/k\Delta h \quad (2)$$

where b_0 is a new crystal layer thickness, σ_s is the lateral surface free energy, σ_e is the fold surface free energy, and Δh is the enthalpy of fusion.

For polymer transcrystallization at the fiber surfaces, the second exponential term in Eq. (1) dominates over the first one [27]. Therefore, the growth rate of transcrystals depends on $1/(T\Delta T)$. Fig. 5b is the plot of $\log G$ against $1/(T\Delta T)$. The linear function relationship was found. With a slope of -1.29×10^5, we obtained a K_g of 2.97×10^5. For α-form crystals of polypropylene [27], b_0 is 0.626 nm, T_m^0 is 458 K, Δh is 209 J g^{-1}. From these values and Eq. (2), the value of $\sigma_s\sigma_e$ was estimated to be about 7.47×10^{-4} J^2 m^{-4}. In α-form crystals of polypropylene [27], a typical value of σ_s is 1.1×10^{-2} J m^{-2}. Thus, we obtained σ_e of 6.8×10^{-2} J m^{-2}. This is consistent with the values ($4-11 \times 10^{-2}$ J m^{-2}) obtained for transcrystals of polypropylene induced by carbon or Kevlar fibers [28].

Fig. 6 shows a typical 2-D WAXD pattern and its corresponding integrated radial scan of the only transcrystalline interphase. The intensities of rings in the 2-D WAXD pattern are not circumferentially uniform, demonstrating some preferred orientation. The main peaks of the radial scan located at $2\theta = 14.2°$, 17.1°, 18.7°, 21.1° and 22.2° are indexed as (110), (040), (130), (111) and (041) reflections, respectively, which are based on the α-form monoclinic packing of polypropylene [29,30]. There are additional WAXD reflections at $2\theta = 15.0°$ and 20.2°, unique to γ-form crystals in polypropylene [31], and are indexed as (113) and (117), respectively. The presence of γ-form transcrystals in the CNT fiber/polypropylene composite under atmospheric pressure is very interesting,

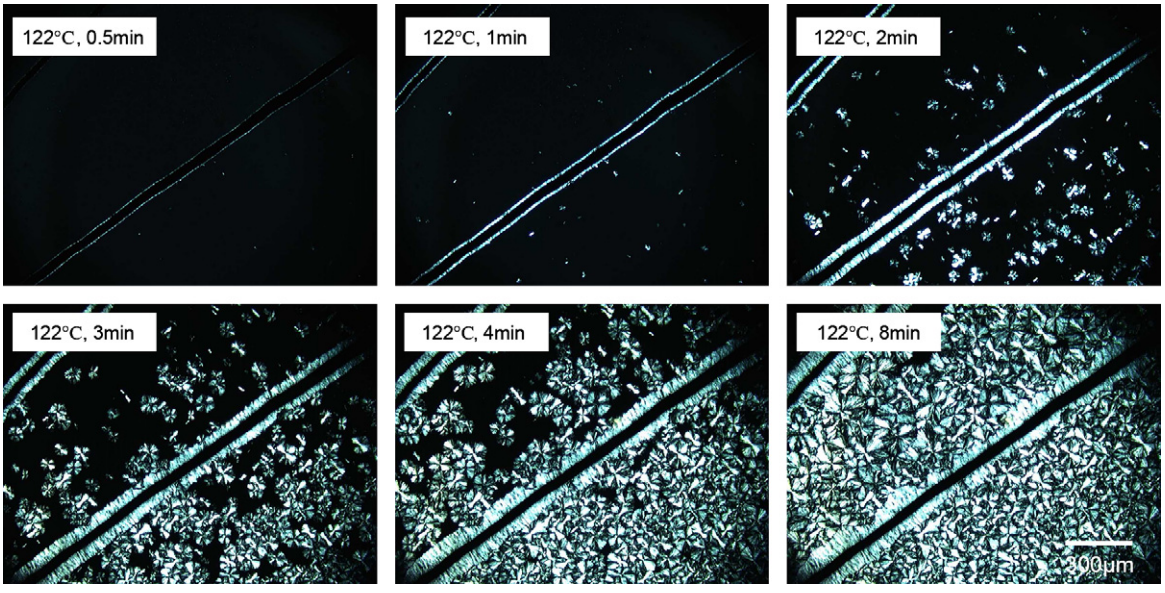

Fig. 4. Optical micrographs under cross-polars of transcrystal developments for polypropylene surrounding the CNT fiber at 122 °C for different times: (a) 0.5 min, (b) 1 min, (c) 2 min, (d) 3 min, (e) 4 min, and (f) 8 min.

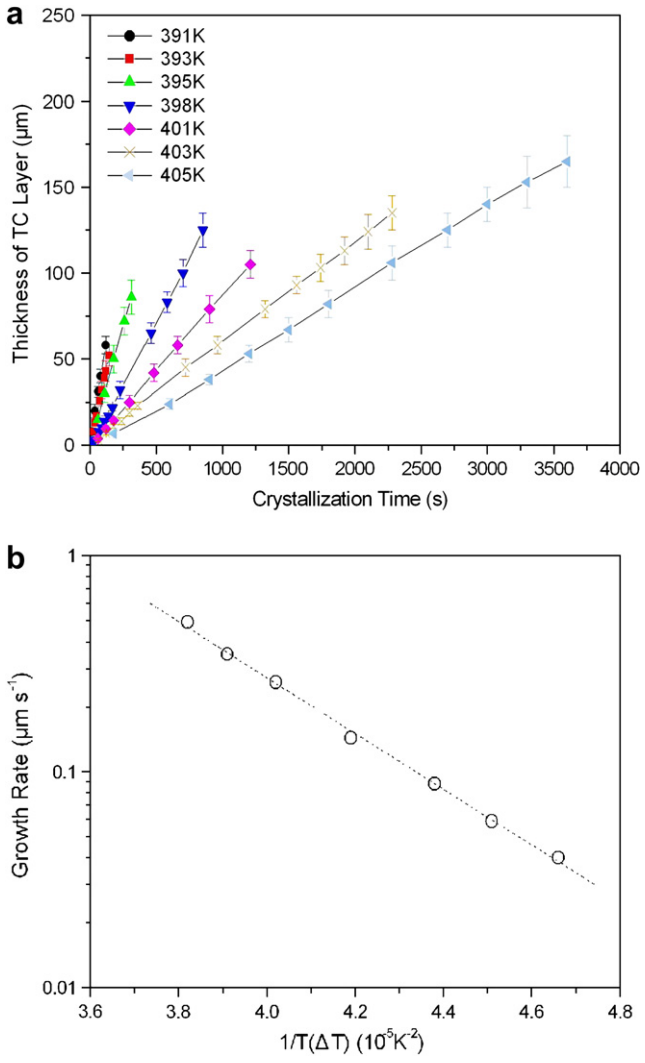

Fig. 5. Kinetics of transcrystallization for polypropylene surrounding the CNT fiber at different isothermal crystallization temperatures: (a) plot of transcrystal thickness against the crystallization time and (b) plot of growth rate of transcrystals against $1/(T\Delta T)$. T is the crystallization temperature, and ΔT, $T_m^0 - T$, is the supercooling degree, where T_m^0 is the equilibrium melting temperature.

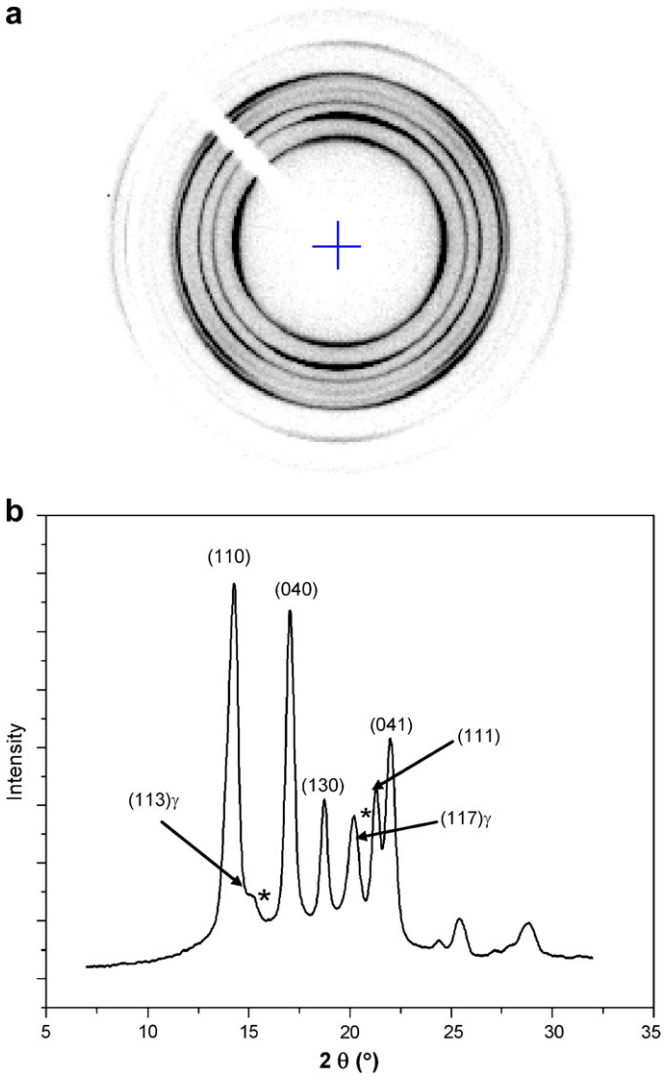

Fig. 6. Wide-angle X-ray diffractions of only transcrystalline interphase region of polypropylene surrounding the CNT fiber: (a) 2-D WAXD pattern and (b) integrated radial scan.

as γ-form crystals are generally observed under high pressure crystallization [32] or under shear-controlled-orientation, for example during injection moulding [33]. Because α-form crystals grow much faster than γ-ones [34,35], the former crystals predominate the overall transcrystalline interphase.

The (110) reflection in our 2-D WAXD patterns consists of four arcs: two equatorial arcs appear stronger than two meridional ones (Fig. 6a). These results demonstrate that two populations of crystalline lamellae develop in the transcrystalline interphase and are typically referred to as the mother and daughter lamellae [29,30,36]. In general, the mother lamellae grow radially outward from the fiber with the *c*-axis parallel to the fiber axis while the daughter lamellae are able to grow on the lateral *ac*-plane of the mother lamellae (Fig. 7) driven by epitaxial matching [29,30,36–38]. The epitaxial angle is about 80° and the resultant microstructure is called cross-hatched lamellar structure [36–38]. As a result, the *b* axes of both mother and daughter lamellae close to the fiber are perpendicular to the fiber (Fig. 7c), where the (040) reflection has two equatorial arcs (Fig. 7a). Transcrystalline layers near and away from the fiber axis were characterized by Marom et al. using synchrotron microbeam X-ray [30]. Results indicated that (040) reflection changed from equator to meridian as one moved away (>50 μm) from the fiber (Fig. 7b). Based on these results, they proposed that both mother and daughter lamellae are away from the fiber twist at 90° around the initial growth direction (Fig. 7d). Our observations on 80 μm thick transcrystalline layers (Fig. 6a) show that (040) reflection is predominantly on the meridian and is consistent with Marom et al.'s observations [30].

Fig. 8 shows SEM images of transcrystalline interphases surrounding the CNT fiber grown at 125 °C after chemical etching. One can clearly see the transcrystalline layer surrounding the CNT fiber and bulk spherulites (Fig. 8a). More details of the lamellar architectures in both transcrystals and bulk spherulites were revealed by higher magnification images

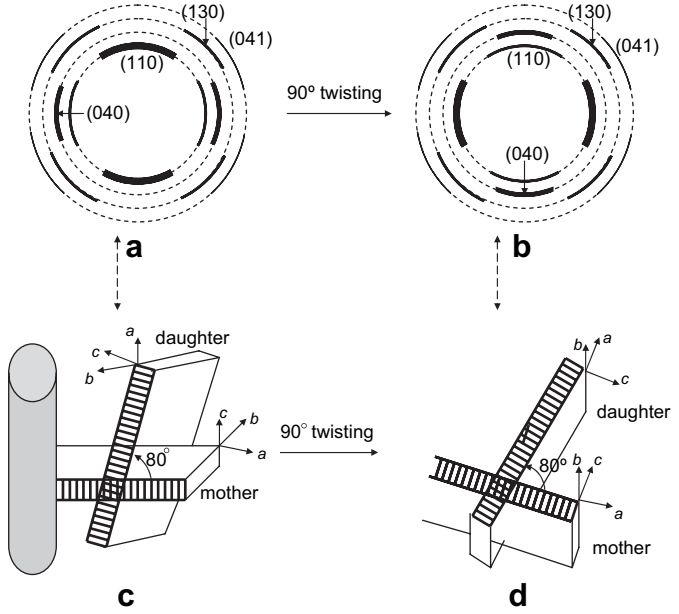

Fig. 7. Schematic illustration of 2-D WAXD patterns of transcrystals and their corresponding microstructure models: (a) and (c) adapted from Refs. [29,30]; (b) and (d) from this study.

(Fig. 8b and c). The lamellar crystals in the transcrystalline interphase are mostly perpendicular to the CNT fiber axis while the lamellae crystals in the bulk spherulites, as expected, grow radially from the nuclei center. The impingement lines between the transcrystals and bulk spherulites were clearly seen at their boundary (Fig. 8d).

Fig. 9a and b shows SEM images of the interfacial morphology adjacent to the CNT fiber surface. The lamellar crystals in the transcrystalline interphase appear as interwoven microstructures. This interwoven morphology is identified as a cross-hatched microstructure. The dominant cross-hatched morphology consists of mother lamellae nucleated on the fiber surface and daughter lamellae epitaxially crystallized on them. This cross-hatched lamellar morphology dominates the whole interfacial zone (about 3–4 μm wide) in the vicinity of the CNT fiber surface. Far away from the CNT fiber, only mother lamellae were observed. These observations indicate a composite microstructure of the transcrystalline interphase. These results are consistent with previous reports of the aramid fiber induced transcrystalline interphase in polypropylene [39,40].

CNTs appear to be wetted by polypropylene (see arrows in Fig. 9a), indicating good interaction between the two. In addition, during solidification, polypropylene matrix shrinks. This results in large spacing between the transcrystalline layer containing few CNTs and rest of the CNT fiber. This is quite evident from Fig. 9b. To further study the adhesive interaction

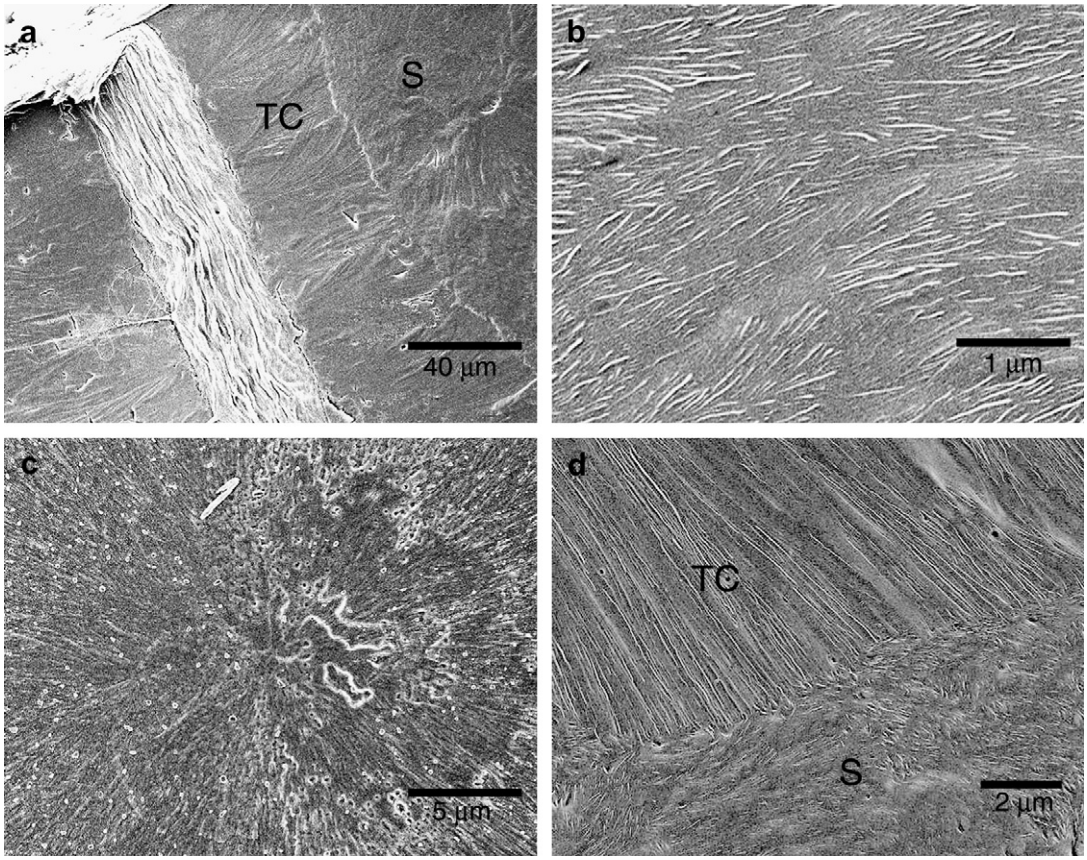

Fig. 8. SEM images of etched transcrystalline interphase regions of polypropylene surrounding the CNT fiber: (a) polypropylene transcrystalline morphology around the single CNT fiber; (b) lamellar microstructure in the transcrystalline layer; (c) lamellar microstructure in the bulk spherulite; and (d) the boundary between transcrystals and spherulites. TC and S represent transcrystals and spherulites, respectively.

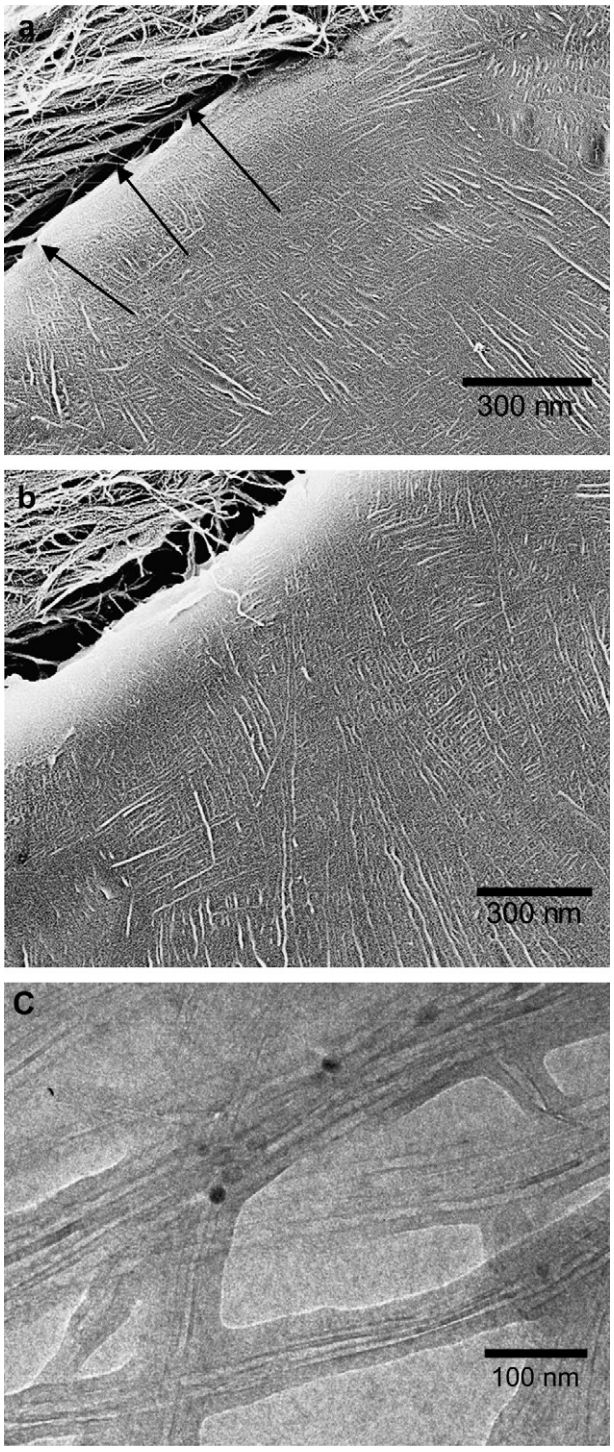

Fig. 9. Cross-hatched microstructures in the etched transcrystalline interphases of polypropylene adjacent to the CNT fiber: (a) and (b) SEM images; (c) TEM bright field image of the CNTs covered by polypropylene. Arrows show wetted CNTs at the transcrystalline interfaces.

between CNTs and polypropylene, a sample was prepared for TEM observation. For this purpose, CNT fibers were suspended in 1,2-dichrolobenzene solution of polypropylene (0.1 wt%). This suspension was maintained at 90 °C for 12 h in a quiescent state [41]. CNT fibers were then pulled out of the solution and heated to 200 °C followed by isothermal crystallization at 125 °C overnight. Finally, polypropylene coated

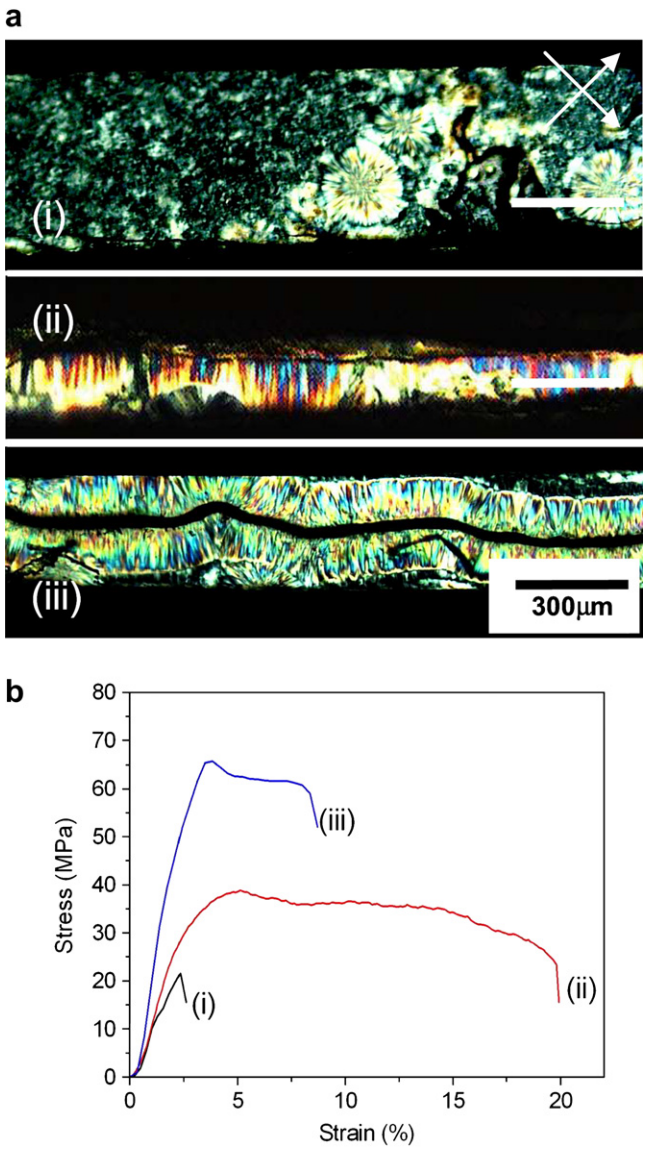

Fig. 10. Mechanical properties of the polypropylene specimens isothermally crystallized at 130 °C overnight: (a) optical images of specimens of control polypropylene (PP), transcrystallized polypropylene (TC-PP) and TC-PP with CNTs (from top to bottom) and (b) stress–strain curves for the specimens.

CNTs were removed from the surface of the CNT fibers using tweezers and placed on the TEM grid. TEM examination (Fig. 9c) confirms that CNTs are well coated with polypropylene.

To study mechanical performance, the rectangular specimens containing only transcrystalline layers with or without the CNT fiber were cut from the films. For comparison, the control polypropylene samples with the same geometry were also prepared and isothermally crystallized under the same conditions. All the samples were crystallized at 130 °C overnight. The optical images of these specimens are shown in Fig. 10a. Mechanical measurements were conducted along the long axis of the rectangular specimens and the data are reported in Fig. 10b and Table 1.

Table 1
Data of mechanical properties of the polypropylene samples isothermally crystallized at 130 °C overnight

Samples[a]	Strength (MPa)	Modulus (GPa)	Elongation to break (%)
Control PP	18 ± 3	1.2 ± 0.1	3.0 ± 0.8
TC-PP	40 ± 2	1.6 ± 0.1	18 ± 3
TC-PP/CNT	60 ± 7	3.3 ± 0.3	7.0 ± 1.6

[a] PP represents polypropylene and TC represents transcrystals.

The control polypropylene had an elongation to break of $3.0 \pm 0.8\%$ with a tensile strength of 18 ± 3 MPa and Young's modulus of 1.2 ± 0.1 GPa. There was no yield point and the samples exhibited brittle fracture. These results are consistent with the previous reports on the crystalline polypropylene with high crystallinity [42–44]. However, transcrystallized polypropylene and transcrystallized polypropylene with CNTs had elongation to break of $18 \pm 3\%$ and $7.0 \pm 1.6\%$, respectively, and the stretching was accompanied by the development of opacity and necking. Such ductile deformation has been reported for the transcrystalline interphase of polypropylene induced by carbon fibers [45]. It is assumed that the daughter lamellae are being unfolded with stretching, which contribute to the large elongation of the transcrystallized polypropylene film [45]. Transcrystallized polypropylene has a tensile strength and modulus of 40 ± 2 MPa and 1.6 ± 0.1 GPa, respectively. Higher modulus of transcrystallized polypropylene as compared to the control polypropylene is attributed to somewhat higher orientation of polymer chains from mother lamellae [16]. Whereas transcrystallized polypropylene with CNTs exhibits further 100% increase in Young's modulus and 50% increase in tensile strength, compared to transcrystallized polypropylene. Therefore, the strength and modulus of transcrystallized polypropylene with CNTs (about 3 wt%) are 200% higher than those of the control polypropylene crystallized by itself (Table 1). The effective load transfer from transcrystallized polypropylene layer to CNTs may contribute to such an improvement.

4. Conclusions

In summary, carbon nanotubes have been shown to act as heterogeneous nucleating agents for polypropylene transcrystallization. Nucleation of polypropylene occurs first at the surface of the carbon nanotube fiber and grows into transcrystals perpendicular to the nanotube fiber axis. By analyzing kinetics of the transcrystallization process using the theory of heterogeneous nucleation, the fold surface free energy of the transcrystals is deduced to be about $6.8 \times 10^{-2}\,\mathrm{J\,m^{-2}}$. We have observed that carbon nanotubes nucleate the growth of both α- and γ-transcrystal, and α-transcrystals dominate the interphase region. Close to the nanotube fiber surface, the mother and daughter lamellae of α-transcrystals form a cross-hatched microstructure with an epitaxial angle of about 80°. Mechanical properties of the transcrystalline layer and that of the transcrystal–nanotube composite are also reported and compared to that of the normally crystallized polypropylene.

Acknowledgements

Financial support from the Air Force Office of Scientific Research is gratefully acknowledged.

References

[1] Baughman RH, Zakhidov AA, de Heer WA. Science 2002;297:787.
[2] Sreekumar TV, Liu T, Min BG, Guo H, Kumar S, Hauge RH, et al. Adv Mater 2004;16:58.
[3] Cadek M, Coleman JN, Ryan KP, Nicolosi V, Bister G, Fonseca A, et al. Nano Lett 2004;4:353.
[4] Ajayan PM, Schadler LS, Giannaris C, Rubio A. Adv Mater 2000;12:750.
[5] Shaffer MSP, Windle AH. Adv Mater 1999;11:937.
[6] Frankland SJ, Caglar A, Brenner DW, Griebel M. J Phys Chem B 2002;106:3046.
[7] Wagner HD, Lourie O, Feldman Y, Tenne R. Appl Phys Lett 1998;72:188.
[8] Lian K, Li S. Appl Phys Lett 2001;79:4225.
[9] Schadler LS, Giannaris SC, Ajayan PM. Appl Phys Lett 1998;73:3842.
[10] Varga J, Karger-Kocsis J. Polymer 1995;36:4877.
[11] Amitax-Sadovsky E, Zheng S, Smith J, Wagner HD. Acta Polym 1998;49:588.
[12] Hobbs SY. Nat Phys Sci 1971;234:12.
[13] Incardona SD, Dimaggio R, Fambril L, Migliaresi C, Marom G. J Mater Sci 1993;28:4983.
[14] Zhang M, Xu J, Zhang Z, Zeng H, Xiong X. Polymer 1996;37:5151.
[15] Chen EJH, Hsiao BS. Polym Eng Sci 1992;32:280.
[16] Quan H, Li ZM, Yang MB, Huang R. Compos Sci Technol 2005;65:999.
[17] Heppenstall-Butler M, Bannister DJ, Young RJ. Composites Part A 1996;27:833.
[18] Gao SL, Kim JK. Composites Part A 2000;31:517.
[19] Wang C, Liu CR. J Polym Sci Part B Polym Phys 1998;36:1361.
[20] Sandler J, Broza G, Nolte M, Schulte K, Lam YM, Shaffer MSP. J Mater Sci 2003;42:479.
[21] Bhattacharyya AR, Sreekumar TV, Liu T, Kumar S, Ericson LM, Hauge RH, et al. Polymer 2003;44:2373.
[22] Li L, Li CY, Ni C. J Am Chem Soc 2006;128:1692.
[23] Chae HG, Minus ML, Kumar S. Polymer 2006;47:3494.
[24] Minus ML, Chae HG, Kumar S. Polymer 2006;47:3705.
[25] Zhu LB, Hess DW, Wong CP. J Phys Chem B 2006;110:5445.
[26] Bassett DC, Olley RH. Polymer 1984;25:935.
[27] Clark EJ, Hoffman JD. Macromolecules 1984;17:878.
[28] Assouline E, Pohl S, Fulchiron R, Gerard JF, Lustiger A, Wagner HD, et al. Polymer 2000;41:7843.
[29] Dean DM, Rebenfeld L, Register RA. J Mater Sci 1998;33:4797.
[30] Assouline E, Wachtel E, Grigull S, Lustiger A, Wagner HD, Marom G. Polymer 2001;42:6231.
[31] Bruckner S, Meille SV. Nature 1989;340:455.
[32] Kalay G, Zhong Z, Allan P, Bevis MJ. Polymer 1996;37:2077.
[33] Campbell RA, Phillips PJ, Lin JS. Polymer 1993;34:4809.
[34] Thomann R, Wang C, Kressler J, Mulhaupt R. Macromolecules 1996;29:8425.
[35] Dean DM, Register RA. J Polym Sci Part B Polym Phys 1998;36:2821.
[36] Binsbergen FL, Delange BGM. Polymer 1968;9:23.
[37] Sauer JA, Morrow DR, Richards GC. J Polym Sci Polym Lett 1965;3:463.
[38] Lotz B, Wittmann JC. J Polym Sci Part B Polym Phys 1986;24:1541.
[39] Kitayama T, Utsumi S, Hamada H, Nishino T, Kikutani T, Ito H. J Appl Polym Sci 2003;88:2875.
[40] Sukhanova TE, Lednicky F, Urban J, Baklagina YG, Mikhailov GM, Kudryavtsev VV. J Mater Sci 1995;30:2201.
[41] Zhang SJ, Kumar S. Macromol Rapid Commun, in press. doi:10.1002/marc.200700838. In this reference, it was shown that polypropylene was crystallized on CNTs in 1,2-dichlorobenzene at 84 °C. CNTs

appeared to precipitate at the higher temperature. In this work, we set the solution crystallization temperature at 90 °C to increase the efficiency of crystallization. CNT precipitation is not an issue in this case as we are starting with CNT fibers.

[42] Alberola N, Fugier M. J Mater Sci 1995;30:860.

[43] Rolando RJ, Krueger WL, Morris HW. Plast Rubber Proc Appl 1989;11:135.

[44] Rolando RJ, Krueger WL, Morris HW. Plast Rubber Proc Appl 1988;10:245.

[45] Hata T, Ohsaka K, Yamada T. J Adhes 1994;45:125.